# Noise spectroscopy with large clouds of cold atoms

Samir Vartabi Kashanian, Aurélien Eloy, William Guerin, Michel Lintz, Mathilde Hugbart, Robin Kaiser

# Noise spectroscopy with large clouds of cold atoms

Samir Vartabi Kashanian[1,2], Aurélien Eloy[1], William Guerin[1], Michel Lintz[2], Mathilde Fouché[1],* and Robin Kaiser[1]
[1] *Université Côte d'Azur, CNRS, INLN, France and*
[2] *Université Côte d'Azur, OCA, CNRS, ARTEMIS, France*
(Dated: June 24, 2016)

Noise measurement is a powerful tool to investigate many phenomena from laser characterization to quantum behavior of light. In this paper, we report on intensity noise measurements obtained when a laser beam is transmitted through a large cloud of cold atoms. While this measurement could possibly investigate complex processes such as the influence of atomic motion, one is first limited by the conversion of the intrinsic laser frequency noise to intensity noise via the atomic resonance. We show that a simple model, based on a mean-field approach, which corresponds to describing the atomic cloud by a dielectric susceptibility, is sufficient to understand the main features of this conversion observed in the experimental intensity noise spectrum.

## I. INTRODUCTION

Progress in the study of light-matter interaction has opened the way to important developments in quantum optics. In particular, laser-cooled atoms are used to develop quantum memories [1], novel laser designs [2, 3], or to prepare non classical states for potential use in metrology [4, 5]. To investigate the nonclassical behavior of light, the study of average intensities is not sufficient and one needs to measure coincidence rates [6, 7], correlation and anticorrelation functions [7–11] or noise and fluctuations [12–15]. Measuring the light fluctuations and correlations after their interaction with cold atomic samples also provides information on the atomic motion [16–18] and could be used to characterize more subtle effects due to interference effects in multiple scattering [19] or obtain direct evidence of the random laser operation in cold atoms [20].

In this kind of experiments, the intrinsic noise of the involved lasers may contribute to the studied fluctuations, and this technical noise may be hard to distinguish from the noise under study. One particular problem is the frequency or phase noise of the laser, which is converted to intensity noise through the atomic resonance in a nontrivial way.

In this work, we study this conversion in detail, by addressing a particular configuration, in which intensity noise measurements are performed on a laser beam *transmitted* through a sample of laser-cooled atoms. This transmission geometry is relevant to investigate different properties, such as the reduction of the noise below the shot-noise level (squeezing) [21, 22], the extra noise due to the atomic internal structure via Raman scattering [23], or two-photon optical nonlinearity [11]. This configuration allows us to use a simple model of light-atom interaction, in which the atomic cloud is described by a complex index of refraction. We show that this 'mean-field approach' [24] is sufficient to explain, qualitatively and quantitatively, the measured power spectral density of the intensity noise after transmission through the cold atomic cloud, even when the on-resonance optical density is large.

The paper is organized as follows. We first present the characterization of our probe laser with standard techniques such as a beat note to measure the optical spectrum and the corresponding linewidth, and the measurement of the frequency noise power spectral density (FNPSD) using the resonance of a Fabry-Perot cavity to convert frequency noise into intensity noise (Sec. II). In Sec. III, the FNPSD is measured using the atomic transition of the laser-cooled vapor as a frequency discriminator. Whereas all the PSD spectra collapse onto the same curve at low Fourier frequencies, some differences appear at higher Fourier frequencies when the probe beam is detuned by various amonts from the center of the resonance line. In order to understand this behavior, we have developed a simple model based on the cloud refractive index. The comparison between experimental results and the predictions of this model shows a very good agreement.

## II. NOISE SPECTROSCOPY WITH A FABRY-PEROT CAVITY

In many experiments, specifically in experiments dealing with noise measurements, it is important to first characterize the intrinsic noise of the laser source. Its spectral properties can be described through the optical spectrum and the corresponding linewidth or through the frequency noise power spectral density. The two approaches are complementary but, while the first one is convenient to quickly compare different types of lasers, the second one gives a much more complete knowledge of the laser spectral properties.

In this section, we present the optical spectrum and FNPSD measurements, using a Fabry-Perot cavity, of a distributed-feedback (DFB) laser. This laser, used for the MOT beams in our cold atom experiment, is amplified by a tapered amplifier (TA). The laser frequency is set close to the $F = 3 \rightarrow F' = 4$ hyperfine component of the D2 resonance line of $^{85}$Rb and locked using a master/slave configuration with an offset locking scheme [25].

*Electronic address: mathilde.fouche@inln.cnrs.fr

### A. Line shape and linewidth

The optical spectrum corresponds to the power spectral density (PSD) of the laser electric field $S_E(\nu)$. It is measured using a beat-note technique sketched in Fig. 1. The beat-note signal is obtained using two different lasers. The first one is the DFB laser we want to characterize. For the second laser we have used a DL Pro commercial external-cavity diode laser (ECDL) from TOPTICA, whose linewidth is specified to be lower than 500 kHz [49]. The lasers are independently frequency locked and the frequency difference between them is typically 1 GHz. The two lasers are injected into a 50 : 50 fiber coupler. The beat-note signal is then detected by a 9.5 GHz bandwidth photodiode and its power spectral density is measured by a spectrum analyzer.

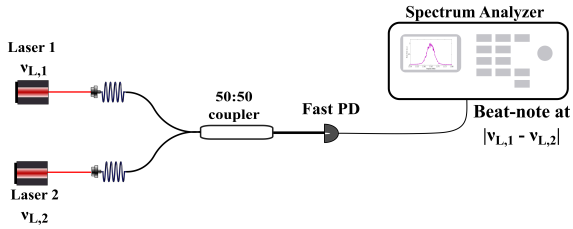


FIG. 1: Setup for the beat-note measurement. Two laser beams are injected in a 50 : 50 coupler. Both lasers are independently frequency locked, and the frequency difference between them is typically 1 GHz. The interference signal is collected by a fast photodiode (PD) and then analyzed by a spectrum analyzer.

The beat-note PSD is plotted in Fig. 2. It corresponds to the convolution of the optical spectrum of the two lasers, but since the linewidth of the TOPTICA laser is much smaller than the DFB laser one, it is mainly dominated by the DFB optical spectrum. It contains a central part at the frequency difference of the two lasers, which can be fitted by a Gaussian, superposed on large wings, which can be fitted by a Lorentzian. The linewidth, given by the full width at half-maximum (FWHM) of the gaussian part, is $\Delta\nu_{\mathrm{BN}} \simeq 3$ MHz. The Lorentzian part has a FWHM of 20 MHz and an amplitude typically one thousand times smaller than the Gaussian part.

Due to the convolution of the two laser Gaussian optical spectra, the square of the beat-note FWHM is the quadratic sum of the two laser linewidths $\Delta\nu_{\mathrm{L}}$:

$$\Delta\nu_{\mathrm{BN}}^2 = \Delta\nu_{\mathrm{L},1}^2 + \Delta\nu_{\mathrm{L},2}^2. \tag{1}$$

To deduce each laser linewidth, three different beat-note signals from three different lasers are needed. The third one is a homemade, etalon-based ECDL with an intermediate linewidth [26]. The results are summarized in Tab. I. The uncertainties are given at $1\sigma$ and have been obtained with a statistical analysis of different beat-note signals recorded in the same conditions.

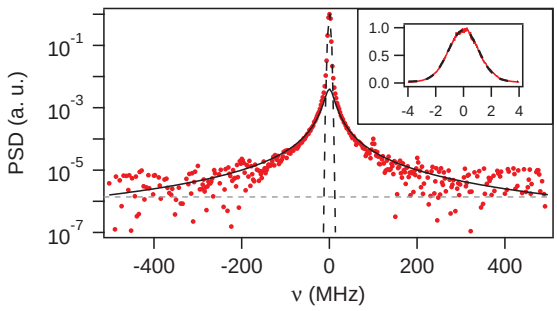


FIG. 2: Beat-note signal PSD between the DFB laser and the TOPTICA laser. The PSD has been averaged 100 times with a sweep time of 0.5 s. The center of the spectrum has been shifted to the origin. Since the TOPTICA laser has a much smaller linewidth than the DFB laser one, it can be treated as a reference laser and the PSD mainly corresponds to the optical spectrum of the DFB laser. The central part can be fitted by a Gaussian (dashed line) with a FWHM $\Delta\nu_{\mathrm{BN}} \simeq 3$ MHz, and the wings are well fitted by a Lorentzian (solid line). The horizontal grey dashed line corresponds to the typical noise floor. Inset: zoom on the Gaussian part of the optical spectrum. Red curve: beat-note signal PSD. Dashed curve: Gaussian fit.

| Laser | Linewidth |
|---|---|
| TOPTICA | $0.2\,(+1.5/-0.2)$ MHz |
| homemade ECDL | $1.1\,(\pm 0.3)$ MHz |
| DFB | $3.0\,(\pm 0.2)$ MHz |

TABLE I: Laser linewidth measured using the beat-note setup, with lasers independently frequency locked. The uncertainties are given at $1\sigma$.

### B. Frequency noise PSD

The laser FNPSD $S_{\nu_{\mathrm{L}}}(f_{\mathrm{n}})$ can be measured using a frequency discriminator that converts frequency noise into intensity noise. One of the most common frequency discriminator is the Fabry-Perot (FP) cavity, whose transmission depends on the light frequency. For a laser linewidth smaller than the cavity linewidth $\Delta\nu_{\mathrm{c}}$, the conversion between the FNPSD and the normalized intensity noise PSD (INPSD) of the transmitted beam is

$$S_{I_{\mathrm{n}}} = \left(\frac{\mathrm{d}T_{\mathrm{c}}}{\mathrm{d}\nu_{\mathrm{L}}}\right)^2 S_{\nu_L}, \tag{2}$$

with $T_{\mathrm{c}}$ the cavity transmission, $\nu_{\mathrm{L}}$ the central laser frequency and $S_{I_{\mathrm{n}}}$ the PSD of the transmitted intensity normalized by the incident intensity. The parameter $D = \mathrm{d}T_{\mathrm{c}}/\mathrm{d}\nu_{\mathrm{L}}$ is the discriminator slope. The optimum conversion is obtained when the laser is tuned to the half maximum of the cavity resonance, where $D$ reaches its maximum $1/\Delta\nu_{\mathrm{c}}$.

The experimental setup is shown in Fig. 3. We use a free-running confocal FP cavity with a length $L_{\mathrm{c}} \simeq 10$ cm. The corresponding free spectral range is $\Delta\nu_{\mathrm{FSR}} =$

$c/4L_c \simeq 750\,\mathrm{MHz}$ and the cavity linewidth is $\Delta\nu_c \simeq 20\,\mathrm{MHz}$. A piezoelectric transducer is placed on one of the mirrors, allowing us to adjust the cavity-to-laser detuning to the half of the cavity resonance. The laser transmitted by the cavity is detected by a homemade transimpedance photodiode and amplified by a low noise AC amplifier. The frequency response of the detection system (photodiode plus amplifier) has been measured by illuminating the photodiode with a shot noise limited thermal light bulb. Its bandwidth ranges from about 10 kHz to 10 MHz. The PSD of the detected signal is recorded by an oscilloscope computing its power spectrum and normalized by the frequency response of the detection system. It is finally converted to frequency noise PSD using Eq. (2).

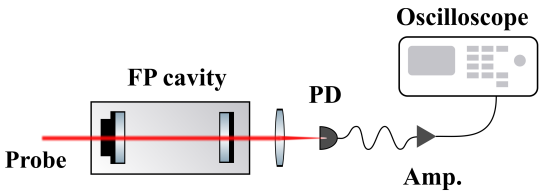


FIG. 3: Schematic of frequency noise PSD measurement using a Fabry-Perot (FP) cavity as a frequency discriminator. PD: photodiode, Amp.: low noise amplifier.

The frequency noise PSD for the DFB laser is depicted in Fig. 4. We have checked that the PSD is not limited by the detection background or by the intrinsic laser intensity noise. The FNPSD essentially decreases as $1/f_n$ up to 1 MHz, corresponding to a flicker noise.

The laser linewidth can be recovered from the frequency noise PSD. The first method is to use the formula which links the FNPSD and the optical spectrum [27]:

$$S_E(\nu) = 2\int_{-\infty}^{\infty} e^{-2i\pi\nu\tau}\left[E_0^2 e^{2i\pi\nu_L\tau} \exp\left(-2\int_0^{\infty} S_{\nu_L}(f_n)\frac{\sin^2(\pi f_n\tau)}{f_n^2}df_n\right)\right]d\tau. \quad (3)$$

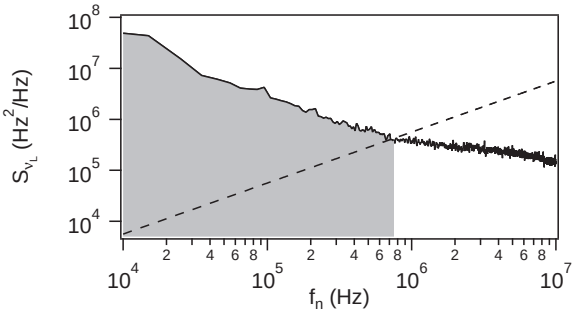


FIG. 4: Frequency noise PSD for the DFB laser. The dashed line corresponds to the $\beta$-separation line used to estimate the laser linewidth. Gray area: contribution to the DFB laser linewidth. See text for further details.

However, most of the time, there is no analytical solution for this equation and one needs to perform a tedious numerical integration. As an alternative method, the laser linewidth can be estimated using a simple geometrical approach, based on the so-called $\beta$-separation line. Since the first theoretical study [28], this approach has been applied in many experimental setups [29–32] and further refined [33, 34].

The $\beta$-separation line is defined as [28]:

$$S_\beta(f_n) = \frac{8\ln(2)}{\pi^2} f_n. \quad (4)$$

This line, plotted in Fig. 4, separates the noise spectrum in two regions. For $S_\beta(f_n) < S_{\nu_L}(f_n)$, frequency noise contributes to the central Gaussian part of the laser line shape and thus to the linewidth. For $S_\beta(f_n) > S_{\nu_L}(f_n)$, frequency noise contributes to the Lorentzian wings of the line shape and does not significantly affect the linewidth. This method approximates the laser linewidth $\Delta\nu_L$, corresponding to the FWHM of the central part of the line shape, by

$$\Delta\nu_L = \sqrt{8\ln(2)A}, \quad (5)$$

with $A$ the area below $S_{\nu_L}$ in the frequency range where $S_{\nu_L}$ is above the $\beta$-separation line, i.e.:

$$A = \int_{1/T_{obs}}^{+\infty} H\left[S_{\nu_L}(f_n) - S_\beta(f_n)\right] S_{\nu_L}(f_n)\mathrm{d}f_n, \quad (6)$$

where $T_{obs}$ is the observation time, and $H$ is the Heaviside step function.

Applying this approach, we obtain a linewidth of $3.4 \pm 0.4\,\mathrm{MHz}$ for the DFB laser. The 10 % relative uncertainty takes into account the maximum typical error introduced by the $\beta$-line approach [33], which is an approximate method to estimate the laser linewidth. The laser linewidth is compatible with the one obtained from the beat-note measurement.

## III. NOISE SPECTROSCOPY WITH COLD ATOMS

The FNPSD presented in the previous section has been measured using a Fabry-Perot cavity as a frequency discriminator. For a free running FP cavity, the results correspond to the convolution of the laser and the cavity resonance frequency noise. While the cavity frequency noise is negligible for noisy lasers, it can become significant when the measurements are performed with narrow lasers. One solution is to use ultra stable cavities [35]. Alternatively, one can also use a molecular or atomic transition as the frequency discriminator. This has been first reported in [36] and then extensively studied theoretically [37–39] as well as experimentally, either to measure the laser properties [40, 41], to extract atomic characteristics [42, 43] or to study the light-matter interaction [44–47].

Frequency noise measurements with an atomic transition are usually done using room temperature or hot vapors. The Doppler effect should be taken into account and limits the atomic spectral linewidth. On the other hand, cold atomic samples correspond to a system where the Doppler effect can generally be ignored, which improves the frequency to intensity noise conversion by reducing the atomic spectral linewidth. We describe in this section our measurements with laser-cooled $^{85}$Rb.

### A. Apparatus

The experimental setup, based on measuring the intensity noise of a weak probe beam transmitted through a cloud of cold atoms, is depicted in Fig. 5a. The atomic cloud is obtained by loading a magneto-optical trap (MOT) with $^{85}$Rb atoms. A compression is applied to increase the atomic density [48]. The maximum number of atoms is $N \simeq 10^{10}$ with a temperature of about 100 $\mu$K and a cloud rms radius of $R \simeq 1$ mm.

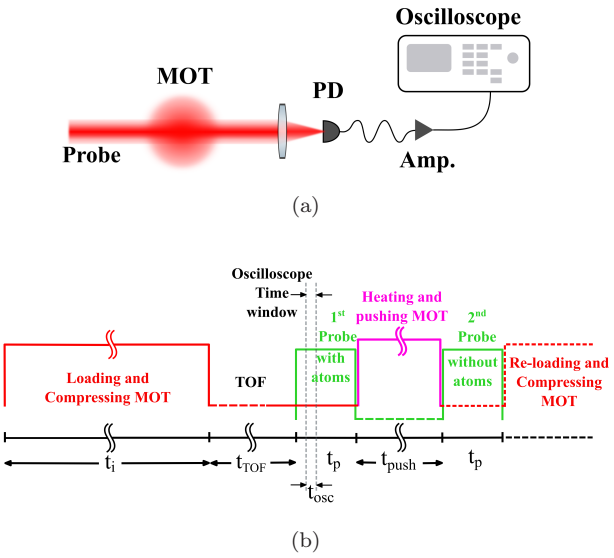


FIG. 5: (a) Schematic of our noise detection setup. PD: photodiode, Amp.: low noise amplifier. (b) Experimental time sequence. Typically $10^{10}$ atoms are loaded in the MOT and compressed during $t_\mathrm{i}$. Then the trapping system switches off and atoms are released. Two probe pulses are applied during $t_\mathrm{p} = 1.2$ ms, after a time of flight of $t_\mathrm{TOF} = 4$ ms. The first pulse provides the transmission through the atomic cloud, and the second one allows us to measure the incident intensity without atoms in order to calculate the normalized transmission for each cycle. The atoms are removed by applying the MOT beams at resonance during $t_\mathrm{push} = 6$ ms between the two probe pulses. For the PSD measurements the time window of the oscilloscope is set $t_\mathrm{pause} = 200\,\mu$s after the beginning of the first probe within $t_\mathrm{osc} = 100\,\mu$s.

The probe beam is the one characterized in the previous section, delivered by the DFB laser amplified by the TA and frequency locked close to the $F = 3 \rightarrow F' = 4$ hyperfine transition of the $D_2$ line of $^{85}$Rb. A double-pass acousto-optical modulator (AOM) is used to change the laser detuning $\delta = (\omega_\mathrm{L} - \omega_0)/\Gamma$ from this transition. The parameter $\omega_\mathrm{L}/2\pi = \nu_\mathrm{L}$ is the laser frequency, $\omega_0/2\pi$ the atomic transition frequency and $\Gamma/2\pi = 6.07$ MHz the natural transition linewidth. The laser beam inside the atomic cloud is linearly polarized and its waist is about 300 $\mu$m. The intensity is adjusted to have a saturation parameter lower than 0.1. The measurements are realized after a fixed $t_\mathrm{TOF} = 4$ ms time of flight (TOF) and the laser beam path has been aligned to correspond to the centre of the atomic cloud after this TOF.

The laser beam after propagation through the atomic cloud is collected by the same homemade photodiode as the one used for the measurements with the FP cavity. This photodiode has two outputs ports. The first port, corresponding to the DC output, is used to measure the probe transmission. The intensity noise is measured thanks to the AC output of the photodiode amplified by a low noise amplifier and connected to the oscilloscope, which computes the intensity noise PSD. As for the measurements done with the FP cavity, the intensity noise PSD is normalized by the frequency response of the detection system. The probe beam is applied during $t_\mathrm{p} = 1.2$ ms but we fix the oscilloscope time window to $t_\mathrm{osc} = 100\,\mu$s, $t_\mathrm{pause} = 200\,\mu$s after the beginning of the probe pulse. To increase the signal to noise ratio, data are integrated over 100 cycles. We also record for each cycle the power of the probe beam without atoms $I_0$, which is needed for intensity to frequency noise conversion. This measurement is done by applying a second probe pulse after having removed all the atoms by shining the MOT beams at resonance during $t_\mathrm{push} = 6$ ms. The time sequence is sketched in Fig. 5b. The duration $t_\mathrm{i}$ includes the loading and compression stages. The optical thickness is varied by changing the total number of atoms through the MOT loading time.

### B. Transmission curve and frequency discriminator

Before noise measurements, we acquire the transmission curve by scanning the laser through the atomic transition. A typical transmission curve is plotted in Fig. 6. The on-resonance optical thickness $b_0$ is extracted by fitting the data by the expected transmission,

$$T \equiv \frac{I_\mathrm{a}}{I_0} = e^{-b(\delta)}, \tag{7}$$

with

$$b(\delta) = \frac{b_0}{1 + 4\delta^2}. \tag{8}$$

The parameter $I_\mathrm{a}$ corresponds to the power measured with atoms while $I_0$ is measured without atoms.

The dependance of the transmission with the laser frequency allows us to use it as a frequency discriminator. The relation between the PSD $S_T$ in [Hz$^{-1}$] of the

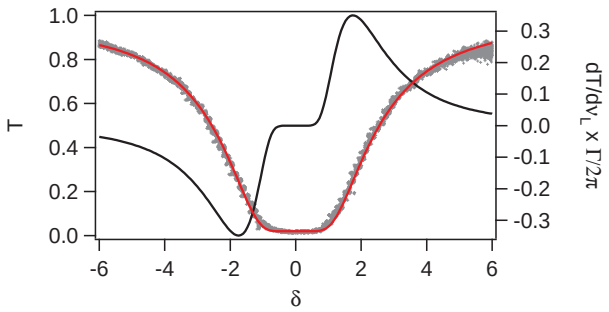


FIG. 6: Grey curve: experimental probe transmission as a function of the laser detuning. Red curve: fit of the transmission curve, giving an on-resonant optical thickness of 19. Black curve: fit derivative used for the intensity to frequency noise conversion (right axis).

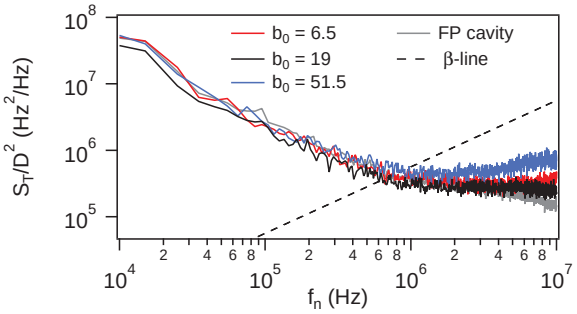


FIG. 7: Laser transmission noise PSD $S_T$ divided by the square of the discriminator slope $D^2$, measured using a cold atomic cloud as a frequency discriminator. For low Fourier frequencies, Eq. (9) is valid and the curves thus correspond to the laser frequency noise PSD. The frequency noise PSD measured with the Fabry-Perot cavity is plotted in grey. The $\beta$-line corresponds to the dashed line.

transmitted intensity normalized by the intensity without atoms, $T = I_a/I_0$, and the laser frequency noise PSD $S_{\nu_L}$ in $[\mathrm{Hz}^2/\mathrm{Hz}]$ is given by the following equation,

$$S_T = \left(\frac{\mathrm{d}T}{\mathrm{d}\nu_L}\right)^2 S_{\nu_L} \quad (9)$$

$$= D^2 S_{\nu_L}, \quad (10)$$

valid when the transmission curve can be locally approximated by a line whose slope is equal to $D$. As we will see in Sec. III D, this is a good approximation for low Fourier frequencies. Using Eqs. (7) and (8), one finds:

$$D = \frac{\mathrm{d}T}{\mathrm{d}\nu_L} = \frac{16\pi\delta b_0}{\Gamma\left(1+4\delta^2\right)^2} e^{-\frac{b_0}{1+4\delta^2}}. \quad (11)$$

The discriminator slope depends on the optical thickness $b_0$ as well as the laser detuning $\delta$. A typical curve is plotted in Fig. 6 for an optical thickness of 19. The best conversion is obtained when $|D|$ is maximum, corresponding to $|\delta| \simeq 1.8$ for $b_0 = 19$.

### C. Experimental results

We have measured the transmitted intensity noise PSD for three different on-resonance optical thicknesses: $b_0 = 6.5$, 19 and 51.5. For each $b_0$, the laser detuning is adjusted, thanks to the double-pass AOM, to be at the maximum of the discriminator slope on the blue side of the atomic transition. We have first checked that the intrinsic laser intensity noise, measured without atoms, is well below the intensity noise PSD measured with atoms. The PSD $S_T$ is then converted to frequency noise PSD using Eq. (9).

The results are plotted in Fig. 7 for the three optical thicknesses. The frequency noise obtained via the Fabry-Perot cavity is also plotted together with the $\beta$-separation line. Whereas all the PSD are consistent at low frequencies, typically below 1 MHz, some differences appear at higher frequencies.

#### 1. *Frequency noise at low frequencies*

For low Fourier frequencies, typically for $f_n$ below 1 MHz, Eq. (9) is valid and the curves plotted in Fig. 7 thus correspond to the laser frequency noise PSD. As done previously with the FP cavity, we can extract the laser linewidth using the $\beta$-separation line approach. The values are listed in Table II together with the values obtained with the Fabry-Perot cavity and with the beat-note measurements. The uncertainties obtained with the cold atomic cloud take into account the statistical uncertainty (standard deviation of the linewidth measurements obtained in similar conditions) as well as the estimation of the maximum error due to the $\beta$-separation line approach [33].

| Experimental technique | Linewidth |
|---|---|
| Beat-note | $3.0 \pm 0.2$ MHz |
| FP cavity | $3.4 \pm 0.4$ MHz |
| Cold atomic cloud | |
| $b_0 = 6.5$ | $3.7 \pm 0.5$ MHz |
| $b_0 = 19$ | $3.3 \pm 0.5$ MHz |
| $b_0 = 51.5$ | $3.7 \pm 0.5$ MHz |

TABLE II: DFB laser linewidth obtained with different techniques.

#### 2. *Frequency noise at high frequencies*

We can see in Fig. 7 that the PSDs differ at high frequencies, with in particular the appearance of a small "bump". However, these curves becomes limited by the noise floor of the photodiode for frequencies higher than 1 MHz. To overcome this problem, the photodiode and the amplifier have been replaced by a new photodiode,

with a high cutoff frequency of 240 MHz and with a lower noise floor.

Typical FNPSDs, obtained with this low noise photodiode, are zoomed at high frequencies in Fig. 8. The three curves have been measured with the same optical thickness $b_0 = 19$ but for three different laser detunings. We clearly see the appearance of bumps whose frequency positions depend on the laser detuning. These positions also depend on the optical thickness as shown in Fig. 10, where the frequency position of the first and second bump is plotted as a function of the laser detuning and for the three previous optical thicknesses.

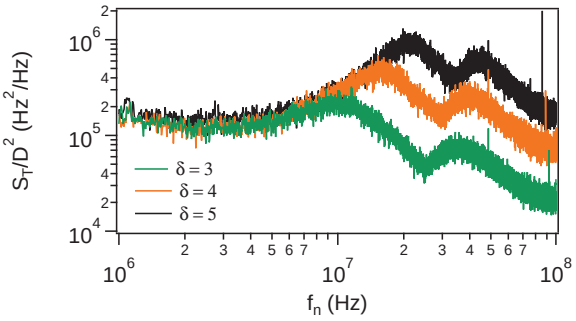


FIG. 8: Zoom at high Fourier frequencies of the laser transmission noise PSD $S_T$ divided by the square of the discriminator slope $D^2$ using a cold atomic cloud with an optical thickness of $b_0 = 19$ and for three different laser detunings.

### D. Modeling

To understand what happens at high frequencies, we model the laser frequency noise as a carrier at frequency $\nu_L$ with two weak sidebands at $\nu_L \pm f_n$ as done in Ref. [46]. It corresponds to a phase modulation where the laser field can be written as follows:

$$E = E_0 e^{i[2\pi\nu_L t + B\sin(2\pi f_n t)]}, \quad (12)$$

$$\simeq E_0\left[e^{i2\pi\nu_L t} + \frac{B}{2}e^{i2\pi(\nu_L+f_n)t} - \frac{B}{2}e^{i2\pi(\nu_L-f_n)t}\right] \quad (13)$$

The parameter $B$ corresponds to the phase modulation depth. The corresponding amplitude of the frequency noise at frequency $f_n$ is $Bf_n$.

When the laser goes through the atoms, the carrier and the two sidebands experience different transmissions $\sqrt{T}$ and phase shifts $\phi$:

$$\sqrt{T(\delta)} = e^{-\frac{b_0}{2(1+4\delta^2)}}, \quad (14)$$

$$\phi(\delta) = -\frac{b_0\delta}{1+4\delta^2}. \quad (15)$$

The laser intensity transmission as a function of time $t$ becomes

$$\frac{I_a}{I_0} = T_0\left[1 + \frac{BC}{\sqrt{T_0}}\cos(2\pi f_n t + \psi)\right], \quad (16)$$

where $\psi$ is a phase shift and

$$C = \sqrt{T_1 + T_2 - 2\sqrt{T_1 T_2}\cos(2\phi_0 - \phi_1 - \phi_2)}, \quad (17)$$

where $T_0$ and $\phi_0$ are the intensity transmission and phase shift induced by the atoms on the carrier and $T_1$, $T_2$, $\phi_1$, $\phi_2$ the intensity transmission and phase shifts induced on the two sidebands. The theoretical frequency to intensity noise conversion is thus given by:

$$S_{T,\mathrm{th}} = \left(\frac{\delta I_a}{I_0}\right)^2 = T_0\frac{C^2}{f_n^2}S_{\nu_L}. \quad (18)$$

We can show that we recover the conversion given by Eqs. (9) and (11) for $f_n \ll \Gamma$ and $f_n \ll \delta\Gamma$ respectively.

This model is used to calculate the expected noise of the transmitted intensity. We assume a white frequency noise for frequencies higher than 1 MHz. Its value, extracted from the measured PSD at $f_n = 1$ MHz, is set to $(Bf_n)^2 \simeq S_{\nu_L} \simeq 10^5\,\mathrm{Hz}^2/\mathrm{Hz}$. This is injected in Eq. (18) to calculate the expected transmission noise PSD $S_{T,\mathrm{th}}$. We then divide it by the discriminator slope given by Eq. (11) in order to compare it to the measurements.

Typical calculated and measured PSD are compared in Fig. 9. The optical thickness is $b_0 = 19$ and the laser detuning is $\delta = 3$. We see a good overlap between the measured and the calculated PSD, without any free parameter. In particular, the model predicts the existence of two bumps whose frequency positions correspond to the ones experimentally observed. These bumps are intrinsically related to the fact that we deal with frequency noise. On the contrary, if we do the calculations assuming an incident laser with amplitude noise, one sees the appearance of dips instead of bumps. The presence of bumps or dips is thus a clear signature of the nature of the laser noise.

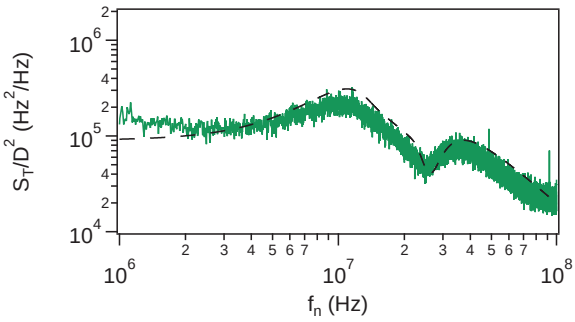


FIG. 9: Solid line: laser transmission noise PSD $S_T$ divided by the square of the discriminator slope $D^2$ using a cold atomic cloud with an optical thickness of $b_0 = 19$ and a laser detuning of $\delta = 3$. Dashed line: $S_{\nu_L,\mathrm{th}}/D^2$ calculated using Eqs. (17) and (18) assuming a white frequency noise.

Finally, we have compared the measured and the calculated bump positions, corresponding to the frequency position of the local maxima, as a function of the laser

detuning and for the three different optical thicknesses. The results are plotted in Fig. 10. We obtain a very good agreement between measurements and calculations, validating the model used to understand the frequency to intensity noise conversion. We can also notice that the frequency difference between both bump positions remains constant, at least for sufficiently high laser detuning, and that this difference roughly corresponds to the frequency range where the transmission curve is close to zero. Both bumps can thus be interpreted as the signature of the beat-note between the carrier and the phase shifted and attenuated sideband that goes from one side of the transmission curve to the other.

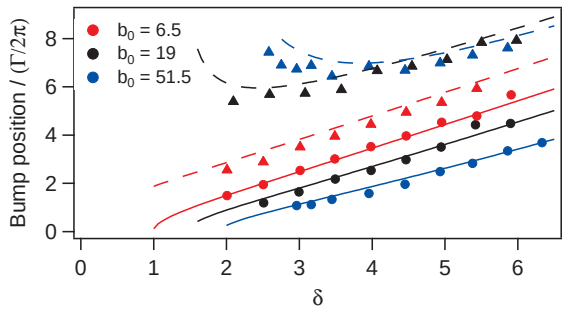


FIG. 10: Points: experimental frequency position of the bumps (circles: first bump, triangles: second bump) observed in the frequency noise PSD, obtained with the cold atomic cloud, as a function of the laser detuning. Solid line: calculated frequency position of the first bump. Dashed line: calculated frequency position of the second bump.

## IV. CONCLUSION

In this paper, we have studied the intensity noise on a laser beam transmitted through a cold atomic cloud. In this forward configuration, we have observed the conversion of the intrinsic laser frequency noise to intensity noise, the atomic transition playing the role of a frequency discriminator whose slope is adjustable through the optical thickness. While we recover the same FNPSD at low Fourier frequencies using a Fabry-Perot cavity, some differences appear at higher Fourier frequencies and one needs to go beyond the linear response approximation of the discriminator given in Eq. (9). We have shown that a simple model in which the frequency noise is modeled as a carrier with two sidebands and the atomic cloud as a medium with an index of refraction is sufficient to describe the observations.

The conversion of the laser frequency noise to intensity noise can be used to characterize the laser noise. Conversely, when the frequency noise is known, its measurement allows extracting information on the discriminator medium itself. We have seen that the frequency positions of the bumps in the FNPSD depend on the laser detuning from the atomic transition and on the optical thickness. One could thus imagine to extract the two last quantities by directly measuring one FNPSD instead of measuring the entire transmission curve by scanning the laser frequency around the atomic transition.

Finally, in the forward direction, the conversion of the intrinsic laser frequency noise to intensity noise is usually an important source of noise. An accurate understanding of this effect is thus of crucial importance. With this conversion now well characterized, intensity noise measurements could possibly be used to extract some signatures of more involved phenomena, such as the observation of the influence of atomic motion and quantum optical properties [11, 21–23].

### Acknowledgments

We thank Gabriel Hétet for the very first measurements on this setup. A. Eloy acknowledges the support of the DGA.

[1] N. Sangouard, C. Simon, H. de Riedmatten, and N. Gisin, Rev. Mod. Phys. **83**, 33 (2011).
[2] W. Guerin, F. Michaud, and R. Kaiser, Phys. Rev. Lett. **101**, 093002 (2008).
[3] J. G. Bohnet, Z. Chen, J. M. Weiner, D. Meiser, M. J. Holland, and J. K. Thompson, Nature **484**, 78 (2012).
[4] O. Hosten, N. J. Engelsen, R. Krishnakumar, and M. A. Kasevich, Nature **529**, 505 (2016).
[5] K. C. Cox, G. P. Greve, J. M. Weiner, and J. K. Thompson, Phys. Rev. Lett. **116**, 093602 (2016).
[6] J. F. Clauser, M. A. Horne, A. Shimony, and R. A. Holt, Phys. Rev. Lett. **23**, 880 (1969).
[7] A. Aspect, J. Dalibard, and G. Roger, Phys. Rev. Lett. **49**, 1804 (1982).
[8] H. J. Kimble, M. Dagenais, and L. Mandel, Phys. Rev. Lett. **39**, 691 (1977).
[9] A. B. U'Ren, C. Silberhorn, J. L. Ball, K. Banaszek, and I. A. Walmsley, Phys. Rev. A **72**, 021802 (2005).
[10] T. Chanelière, D. N. Matsukevich, S. D. Jenkins, S.-Y. Lan, T. A. B. Kennedy, and A. Kuzmic, Nature **438**, 833 (2005).
[11] T. Peyronel, O. Firstenberg, Q.-Y. Liang, S. Hofferberth, A. V. Gorshkov, T. Pohl, M. D. Lukin, and V. Vuletić, Nature **488**, 57 (2012).
[12] C. Silberhorn, P. K. Lam, O. Weiß, F. König, N. Korolkova, and G. Leuchs, Phys. Rev. Lett. **86**, 4267 (2001).
[13] V. Josse, A. Dantan, L. Vernac, A. Bramati, M. Pinard, and E. Giacobino, Phys. Rev. Lett. **91**, 103601 (2003).
[14] A. M. Marino, V. Boyer, and P. D. Lett, Phys. Rev. Lett. **100**, 233601 (2008).

[15] I. H. Agha, G. Messin, and P. Grangier, Opt. Express **18**, 4198 (2010).
[16] C. Jurczak, K. Sengstock, R. Kaiser, N. Vansteenkiste, C. Westbrook, and A. Aspect, Opt. Commun. **115**, 480 (1995).
[17] C. Jurczak, B. Desruelle, K. Sengstock, J. Y. Courtois, C. I. Westbrook, and A. Aspect, Phys. Rev. Lett. **77**, 1727 (1996).
[18] J. A. Grover, P. Solano, L. A. Orozco, and S. L. Rolston, Phys. Rev. A **92**, 013850 (2015).
[19] C. A. Müller, B. Grémaud, and C. Miniatura, Phys. Rev. A **92**, 013819 (2015).
[20] Q. Baudouin, N. Mercadier, V. Guarrera, W. Guerin, and R. Kaiser, Nat. Phys. **9**, 357 (2013).
[21] A. Lambrecht, T. Coudreau, A. M. Steinberg, and E. Giacobino, Europhys. Lett. **36**, 93 (1996).
[22] J. Ries, B. Brezger, and A. I. Lvovsky, Phys. Rev. A **68**, 025801 (2003).
[23] A. Lezama, R. Rebhi, A. Kastberg, S. Tanzilli, and R. Kaiser, Phys. Rev. A **92**, 033853 (2015).
[24] J. Javanainen and J. Ruostekoski, Opt. Express **24**, 993 (2016).
[25] G. Puentes, Appl. Phys. B **107**, 11 (2012).
[26] X. Baillard, A. Gauguet, S. Bize, P. Lemonde, P. Laurent, A. Clairon, and P. Rosenbusch, Opt. Commun. **266**, 609 (2006).
[27] D. S. Elliott, R. Roy, and S. J. Smith, Phys. Rev. A **26**, 12 (1982).
[28] G. D. Domenico, S. Schilt, and P. Thomann, Appl. Opt. **49**, 4801 (2010).
[29] O. Llopis, P. H. Merrer, H. Brahimi, K. Saleh, and P. Lacroix, Opt. Lett. **36**, 2713 (2011).
[30] N. Bucalovic, V. Dolgovskiy, C. Schori, P. Thomann, G. D. Domenico, and S. Schilt, Appl. Opt. **51**, 4582 (2012).
[31] H. Dinesan, E. Fasci, A. D'Addio, A. Castrillo, and L. Gianfrani, Opt. Express **23**, 1757 (2015).
[32] I. Ricciardi, S. Mosca, M. Parisi, P. Maddaloni, L. Santamaria, P. D. Natale, and M. D. Rosa, Opt. Lett. **40**, 4743 (2015).
[33] Q. Zhou, J. Qin, W. Xie, Z. Liu, Y. Tong, Y. Dong, and W. Hu, Appl. Opt. **54**, 8282 (2015).
[34] Q. Zhou, J. Qin, W. Xie, Z. Liu, Y. Tong, Y. Dong, and W. Hu, Opt. Express **23**, 29245 (2015).
[35] B. C. Young, F. C. Cruz, W. M. Itano, and J. C. Bergquist, Phys. Rev. Lett. **82**, 3799 (1999).
[36] T. Yabuzaki, T. Mitsui, and U. Tanaka, Phys. Rev. Lett. **67**, 2453 (1991).
[37] R. Walser and P. Zoller, Phys. Rev. A **49**, 5067 (1994).
[38] I. V. Jyotsna, G. S. Agarwal, and G. Vemuri, Phys. Rev. A **51**, 3169 (1995).
[39] K. V. Vasavada, G. Vemuri, and G. S. Agarwal, Phys. Rev. A **52**, 4159 (1995).
[40] T. L. Myers, R. M. Williams, M. S. Taubman, C. Gmachl, F. Capasso, D. L. Sivco, J. N. Baillargeon, and A. Y. Cho, Opt. Lett. **27**, 170 (2002).
[41] S. Bartalini, S. Borri, P. Cancio, A. Castrillo, I. Galli, G. Giusfredi, D. Mazzotti, L. Gianfrani, and P. De Natale, Phys. Rev. Lett. **104**, 083904 (2010).
[42] R. J. McLean, C. E. Fairchild, P. L. Dyson, and P. Hannaford, Opt. Lett. **18**, 1675 (1993).
[43] M. Rosenbluh, A. Rosenhouse-Dantsker, A. Wilson-Gordon, M. Levenson, and R. Walser, Opt. Commun. **146**, 158 (1998).
[44] D. H. McIntyre, J. Cooper, R. Walser, and C. E. Fairchild, Opt. Lett. **18**, 1816 (1993).
[45] J. C. Camparo and J. G. Coffer, Phys. Rev. A **59**, 728 (1999).
[46] M. Bahoura and A. Clairon, Opt. Lett. **26**, 926 (2001).
[47] J. J. Townsend, J. G. Coffer, and J. C. Camparo, Phys. Rev. A **72**, 033807 (2005).
[48] M. T. DePue, S. L. Winoto, D. Han, and D. S. Weiss, Optics Communications **180**, 73 (2000).
[49] This specification is given for a free-running laser with a measurement time of 5 $\mu$s